Geometric mechanism for antimonotonicity in scalar maps with two critical points

Silvina Ponce Dawson
Laboratory for Plasma Research, University of Maryland, College Park, Maryland 20742

Celso Grebogi
Laboratory for Plasma Research, Institute for Physical Science and Technology, and Department of Mathematics, University of Maryland, College Park, Maryland 20742

Hüseyin Koçak
Department of Mathematics and Computer Science, University of Miami, Coral Gables, Florida 33124
(Received 21 April 1993)

Concurrent creation and destruction of periodic orbits—antimonotonicity—for one-parameter scalar maps with at least two critical points are investigated. It is observed that if, for a parameter value, two critical points lie in an interval that is a chaotic attractor, then, generically, as the parameter is varied through any neighborhood of such a value, periodic orbits should be created and destroyed infinitely often. A general mechanism for this complicated dynamics for one-dimensional multimodal maps is proposed similar to the one of contact-making and contact-breaking homoclinic tangencies in two-dimensional dissipative maps. This subtle phenomenon is demonstrated in a detailed numerical study of a specific one-dimensional cubic map.

PACS number(s): 05.45.+b

I. INTRODUCTION

Bifurcations of periodic points of one-dimensional maps command a prominent place in theoretical and experimental investigations of dynamical systems. For example, the one-parameter quadratic map $x_{n+1}=\alpha-x_n^2$ has been studied as the quintessential example exhibiting one of the most common routes to chaos: period-doubling cascades [1]. Moreover, some of the important bifurcation behaviors of the quadratic map have been found to be universal in a large class of unimodal maps—maps with one critical point [2]. Despite the remarkable success of unimodal maps in modeling bifurcations in many applications [3], they also have inherent limitations. For example, as the parameter α in the quadratic map is increased, it has been shown that periodic orbits are only created but never destroyed [4].

Unlike the monotone bifurcation behavior of the quadratic map, creation and destruction of periodic orbits have been observed both numerically [5] and experimentally [6] in various nonlinear systems. For example, as depicted in Fig. 1, reversals of period-doubling cascades are indeed visible in a numerically computed bifurcation diagram of the Poincaré map of the periodically forced oscillator of Van der Pol, which is prototypical model for many nonlinear oscillatory phenomena. The Poincaré map of this nonlinear oscillator, as well as many others, can be captured by a degree-one circle map, or simply by a scalar multimodal map—a map with several critical points [7]. Indeed, this is one of the reasons why multimodal maps have been the center of different analytical and numerical studies [8].

In this paper we present a geometric mechanism for the creation and destruction of periodic orbits infinitely often as a parameter is increased near certain common parameter values in generic chaotic multimodal scalar maps with at least two critical points. We call such concurrent creation and destruction of periodic orbits *antimonotonicity* [9]. To describe antimonotonicity for multimodal scalar maps more precisely, we proceed with some definitions.

In a one-parameter scalar map $x_{n+1}=F(x_n,\alpha)$, a parameter value $\alpha=\alpha_0$ is called an *orbit creation value* if a periodic orbit does not exist for $\alpha<\alpha_0$ but exists for $\alpha>\alpha_0$. Similarly, $\alpha=\alpha_0$ is called an *orbit destruction value* if a certain periodic orbit exists for $\alpha<\alpha_0$ but it does not exist for $\alpha>\alpha_0$. A map $x_{n+1}=F(x_n,\alpha)$ is said to be *increasing (decreasing) monotone* in an interval J of parameter values if, for $\alpha\in J$, periodic orbits are only

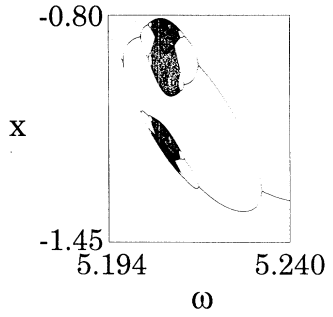

FIG. 1. Reversals of period-doubling cascades in the periodically forced oscillator of Van der Pol $\ddot{x}+5(x^2-1)\dot{x}+x=40\sin(\omega t)$. In this bifurcation diagram, the x coordinate of the Poincaré map is plotted against the driving frequency ω.

created (destroyed). For instance, the quadratic family is increasing monotone on the interval $[-\frac{1}{4},2]$. On the other hand, we say that a family is *antimonotone* at a parameter value α^* if for each $\in>0$ there is creation *and* destruction of periodic orbits in at least one of the intervals $(\alpha^*,\alpha^*+\epsilon)$ or $(\alpha^*-\epsilon,\alpha^*)$. The parameter value α^* is an *antimonotone value.* Antimonotonicity implies the existence of infinitely many orbit creation and infinitely many orbit destruction parameter values in any neighborhood of α^*, a situation with important consequences for experiments on the fine structure of chaotic systems. Indeed, as we have reported in an earlier publication [10], we believe that antimonotonicity is a common phenomenon in one-dimensional chaotic systems: *If a one-dimensional map* $x_{n+1}=F(x_n,\alpha)$ *has at least two critical points that lie in a chaotic attractor for a parameter value* $\alpha=\alpha^*$, *then generically,* F *is antimonotone at* α^*. We shall specify the genericity conditions in detail later in Sec. III. However, we hasten to point out, in particular, that the multimodal map $x_{n+1}=\alpha-\alpha^2+2\alpha x_n^2-x_n^4$, which is the second iterate of the quadratic map, is not generic.

The geometric mechanism—dimple formation—as the source of antimonotonicity presented here is similar to the one in two-dimensional maps. In the case of two-dimensional invertible maps a definite result on antimonotonicity has been proven [9]: Any dissipative C^3 diffeomorphism is antimonotone at a parameter value for which it has a nondegenerate homoclinic tangency. This result is established by proving the concurrency of two types of homoclinic tangencies. A homoclinic tangency is called *contact making* if transversal homoclinic points are created as the parameter is increased; similarly, a homoclinic tangency is called *contact breaking* if some transversal homoclinic points are annihilated locally as the parameter is increased. The source of antimonotonicity in two dimensions is a consequence of the fact that near any parameter value for which there is a contact-making homoclinic tangency there must be a parameter value with a contact-breaking homoclinic tangency. In the one-dimensional case, the dimple formation turns out to be a source of the concurrent contact-making and contact-breaking tangencies.

Although a rigorous proof of antimonotonicity in two dimensions exists, there remains substantial mathematical difficulties which prevent us from providing a complete proof in dimension one for multimodal maps. In the remainder of this paper, we do, however, provide a geometric mechanism which leads us to our main observation. More importantly, we present a careful numerical study of a specific cubic map where the dimple formation as the source of antimonotonicity is indeed visible.

II. A NUMERICAL EXAMPLE

Antimonotonicity is a subtle phenomenon. Yet, it is observable in specific maps with careful numerical computations and thus is of considerable practical importance. In this section we present a specific cubic map exhibiting antimonotonicity. This example is quite general and we believe that it reflects what happens with any gen-

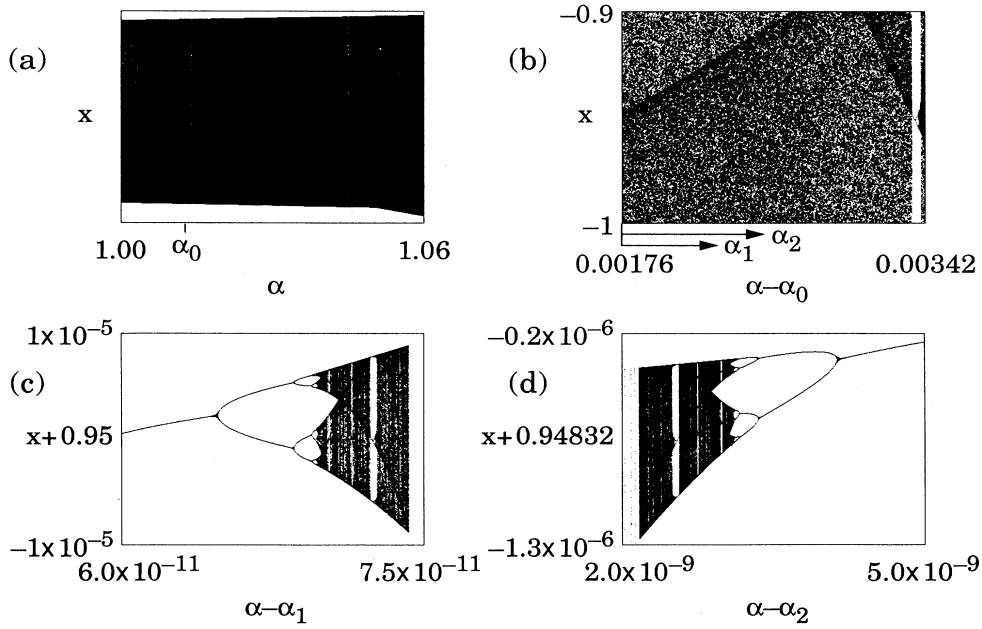

FIG. 2. Bifurcation diagrams of $x_{n+1}=F(x_n,\alpha)\equiv\alpha[-x_n^3+3(0.95)^2x_n]+0.099$. (a) For each $\alpha\in(1.0,1.06)$, the iterates 1000–3000 of the two critical points at ±0.95 are plotted. (b) Enlargement of (a) around the parameter value $\alpha_0=1.03$. (c) Further enlargement of the bifurcation diagram around $\alpha_1=1.031\,763\,203$. The iterates 1400–11 200 of the initial point -0.95 are plotted. Actually, the whole attractor for each value of α is made of 14 pieces similar to the one observed in the figure. Therefore, in this window, orbits of period proportional to 14 are created. (d) Another enlargement of the bifurcation diagram, this time around the parameter value $\alpha_2=1.031\,764\,52$. In this case, the iterates 1500–12 000 of the initial point 0.95 are plotted. The whole attractor for each value of α is made of 15 similar pieces. Therefore, in this window, orbits of period proportional to 15 are destroyed.

eric family of multimodal maps near chaotic parameter values at which the attractor contains two critical points.

Let us consider the scalar cubic map

$$x_{n+1}=F(x_n,\alpha)\equiv\alpha[-x_n^3+3(0.95)^2x_n]+0.099\ , \qquad (1)$$

where α is a scalar parameter. The critical points of F are located at $c_1=0.95$ (a maximum) and $c_2=-0.95$ (a minimum). When α is increased, the critical value $F(c_1,\alpha)$ increases and $F(c_2,\alpha)$ decreases.

We have plotted in Fig. 2(a) the bifurcation diagram of $F(x_n,\alpha)$ for the parameter region $\alpha\in(1.0,1.06)$. In Fig. 2(b), an enlargement of the bifurcation diagram about the parameter value $\alpha=1.03$ is shown. For this parameter value, the critical points are in a chaotic attractor that is an interval. At the moment these bifurcation diagrams do not appear to be informative from the view of bifurcations. However, as we have indicated in the Introduction, we do expect that near $\alpha=1.03$ there should be parameter values at which the periodic orbits are created as α is increased, and parameter values at which periodic orbits are destroyed as α is increased. Indeed, a further enlargement of the bifurcation diagram around $\alpha_1=1.031\,763\,203$ reveals the creation of periodic orbits as seen in Fig. 2(c); in contrast, an enlargement about the parameter value $\alpha_2=1.031\,764\,52$ as depicted in Fig. 3(d) uncovers the annihilation of periodic orbits.

Here, we interrupt the analysis of our example. However, we shall return to it after an explanation of a general geometric mechanism as the source of antimonotonicity in the next section.

III. A GEOMETRIC OUTLINE FOR ANTIMONOTONICITY

In this section we first describe a generic setting for antimonotonicity in one-dimensional maps. Then we outline a geometric mechanism, which we call *dimple formation,* and explain how a dimple formation gives rise to antimonotonicity through homoclinic bifurcations. The computational details of the scenario below will be forthcoming in Sec. V.

The setting. We consider a one-dimensional multimodal map $x_{n+1}=F(x_n,\alpha)$ depending on a parameter α. We require that at a parameter value $\alpha=\alpha^*$, the map F has at least two critical points c_1 and c_2 that are contained in the interior of an interval that is a chaotic attractor. Also, we assume that the chaotic attractor persists for the particular parameter values needed in the discussion below. Finally, we require the orbits of the critical values to be dense in the attractor with a positive Lyapunov exponent.

Homoclinic tangencies. A chaotic attractor as above will always contain an unstable periodic point p, whose preimages (stable set) are dense on the attractor. Since the forward iterates of a critical point c is assumed to be dense on the attractor, we assume that for a parameter value $\hat{\alpha}$ near α^*, the critical point is mapped, after a finite number of iterates, say, n, onto the unstable periodic point p. When this happens the relevant critical point is both on the unstable and on the stable set of p [11]. We call such a parameter value a *homoclinic tangency value.* Moreover, a homoclinic tangency value is said to be *nondegenerate* if the iterate $F^n(c,\alpha)$ of the critical point c crosses past the periodic point with nonvanishing relative velocity, that is, $\partial F^n(c,\hat{\alpha})/\partial\alpha\neq 0$, and F^n has a quadratic extremum at c. Nondegenerate homoclinic tangency values are the parameter values at which homoclinic bifurcations occur: they are points of accumulation of saddle-node and period-doubling bifurcations through which periodic orbits are either created or destroyed [11].

We distinguish two types of nondegenerate homoclinic tangencies. The tangency is *contact making* at $\hat{\alpha}$ if two new preimages of the unstable periodic point under F^n are created immediately after the tangency [10]. In this case, new homoclinic orbits to p are created as α is increased past $\hat{\alpha}$. Analogously, the tangency is *contact breaking* if two preimages of the periodic point are destroyed immediately after the tangency. In this case, homoclinic orbits to p are destroyed as α is increased. Periodic orbits are created for parameter values close to contact-making tangency values and destroyed in the vicinity of contact-breaking ones.

Dimple formation and homoclinic bifurcations. One of the main ingredients that contribute to the occurrence of antimonotonicity is the fact that contact-breaking homoclinic tangencies occur close (in parameter space) to contact-making ones. We now explain how this happens in the case of bimodal map $F(x,\alpha)$.

Since the iterates of the critical points are assumed to be dense on the attractor, for a parameter value α_c near α^*, we expect that $F^m(c_1,\alpha_c)=c_2$ for some iterate of the map while $\partial F^m(c_1,\alpha_c)/\partial\alpha$ is different from zero. At this parameter value, F^{m+1} will have a quartic critical point at c_1. As we vary the parameter further, this quartic critical point spits into three quadratic critical points. Estimates of the relative speeds of these critical points reveal that if, for example, the middle critical point undergoes a contact-breaking homoclinic tangency, the other two critical points undergo contact-making homoclinic tangencies (or vice versa) for nearby parameter values. This geometric mechanism, which we call *dimple formation* is responsible for the creation and annihilation of periodic points for parameter values close to one another.

Antimonotonicity. The final ingredient that contributes to antimonotonicity is the occurrence of infinitely many pairs of contact-making and contact-breaking homoclinic tangencies. Let us consider again the parameter value α^* at which the attractor is chaotic and contains the two critical points c_1 and c_2 in its interior. At that parameter value the union of the unstable periodic orbits and of their preimages are believed to be dense in the attractor. Also, we expect the existence of infinitely many chaotic parameter values near α^*. Therefore, immediately after the dimple is formed at α_c, while the function F^{n+m+1} for some $n+m+1$ is moving as the parameter is varied, we expect the curve $F^{n+m+1}(x,\alpha)$ to typically cross infinitely many preimages or elements of unstable periodic orbits. Accordingly, the family will switch from orbit creation to orbit destruction infinitely often and, thus, will be antimonotone.

As we have mentioned in the introduction, certain nongeneric maps, in particular the second iterate of the

logistic map, do not exhibit antimonotonicity. In the case of unimodal maps with a single critical point c, the parameter values α_c are such that $F^m(c,\alpha_c)=c$, and they are values at which there is a superstable orbit. Therefore, since at $\alpha=\alpha_c$ all points near c are attracted to the superstable orbit, no tangent bifurcations or homoclinic crossings occur in a neighborhood of α_c. For α values close to α_c, there is an attracting periodic orbit and all nearby points are attracted to it. Odd symmetric maps are not generic in the same sense. The other two conditions that are necessary for this picture to hold are the following: (i) $F^m(c_1,\alpha_c)=c_2$ while $\partial F^m(c_1,\alpha_c)/\partial\alpha$ is different from zero. (ii) The nondegeneracy of the homoclinic tangencies, in particular, the condition $\partial^2 F^r(c,\alpha^*)/\partial x^2\neq 0$ for α^* such that $F^r(c,\alpha^*)=p$. We suppose that these are generic conditions.

We will provide the details of computations, supporting the dimple-formation mechanism above, in Sec. V. Next, however, we return to the numerical investigation of our previous specific cubic map and demonstrate that it indeed exhibits dimple formation.

IV. NUMERICAL EXAMPLE CONTINUED

We demonstrate in this section that our previous specific cubic map indeed exhibits the route to antimonotonicity through the dimple formation mechanism outlined above.

The formation of a dimple in the cubic map

$$F(x_n,\alpha)=\alpha[-x_n^3+3(0.95)^2x_n]+0.099$$

as the parameter is increased past $\alpha=\alpha_c$ is shown in Fig. 3. The iterate $F^{13}(x,\alpha)$, with $m=4$ and $n+1=9$, of the map F is plotted as a function of x in a neighborhood of the critical point $c_1=0.95$, for the parameter values $\alpha_c=1.019\,398\,0$, $\alpha_1=1.019\,405\,0$, $\alpha_2=1.019\,411\,0$, $\alpha_3=1.019\,414\,0$, and $\alpha_4=1.019\,416\,0$. The horizontal line indicates the location of a preimage $F^{-k}(p,\alpha)$ for $k=5$ of an unstable fixed point p that is in between c_1 and c_2. Actually, in this example p does depend on α; however, the value of $\partial p/\partial\alpha$ is sufficiently small so that for the range of α values of all the figures that we show, the variation of p is negligible. A dimple is formed to $\alpha=\alpha_c\cong 1.019\,398\,0$ for which $F^m(c_1,\alpha_c)=c_2$, with $m=4$. For $\alpha<\alpha_c$, F^{n+m+1} has only one extremum in the x interval shown, while for $\alpha>\alpha_c$ it has three extrema all moving with positive velocity as the parameter is increased (i.e., $\partial F^{n+m+1}/\partial\alpha>0$ at these extrema). In this way, a contact-making homoclinic tangency occurs at $\alpha=\alpha_2$ and a contact-breaking one at $\alpha=\alpha_3$. Therefore, periodic orbits are created and destroyed for parameter values nearby.

We also illustrate with Fig. 3 some additional pairs of contact-making and contact-breaking homoclinic tangencies that occur for $\alpha\in[\alpha_c,\alpha_4]$. On the right of this figure we have indicated the location of some of the preimages $F^{-k}(p)$ of the unstable fixed point that $F^{13}(c_1,\alpha)$ crosses for these values. We have labeled each of these preim-

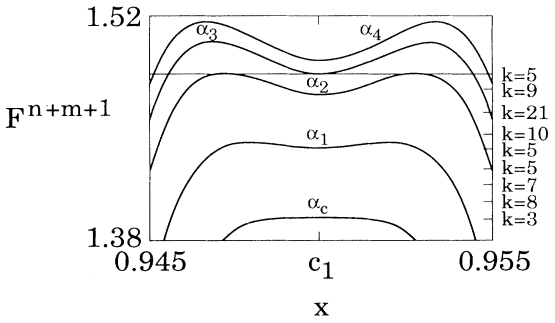

FIG. 3. The creation of a dimple in $x_{n+1}=F(x_n,\alpha)\equiv\alpha[-x_n^3+3(0.95)^2x_n]+0.099$. The iterate $F^{13}(x,\alpha)$ is plotted as a function of x, in a neighborhood of the critical point $c_1=0.95$, for different values of α. The parameter values are $\alpha_c=1.019\,398\,0$, $\alpha_1=1.019\,405\,0$, $\alpha_2=1.019\,411\,0$, $\alpha_3=1.019\,414\,0$, and $\alpha_4=1.019\,416\,0$. The horizontal line indicates the location of a preimage $F^{-k}(p)$ ($k=5$) of the unstable fixed point p. A dimple is formed at $\alpha=\alpha_c\cong 1.019\,398\,0$, when $F^4(c_1)=c_2$. For $\alpha<\alpha_c$, F^{13} has only one extremum in the x interval shown, while for $\alpha>\alpha_c$ it has three, all moving with positive velocity. In this way, a contact-making homoclinic tangency occurs at $\alpha=\alpha_2$ and a contact-breaking one at $\alpha=\alpha_3$. Therefore, periodic orbits are created and destroyed for parameter values nearby. The occurrence of several pairs of homoclinic crossings is also illustrated: on the right of the figure we have indicated the location (at the homoclinic tangency values) of some of the preimages $F^{-k}(p)$ of the unstable fixed point that the curve $F^{n+m+1}(x,\alpha)$ in the x interval shown crosses for $\alpha\in(\alpha_c,\alpha_4]$. The dense occurrence of these pairs of crossings generates antimonotonicity.

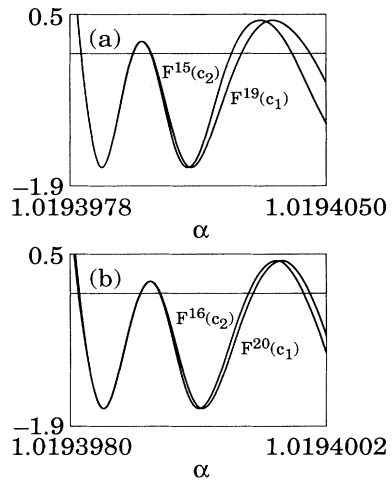

FIG. 4. (a) The iterates $F^{15}(c_2,\alpha)$ and $F^{19}(c_1,\alpha)$ as functions of α for $\alpha\in(\alpha_c,\alpha_1)$, where α_c and α_1 are the same as in Fig. 3. (b) The iterates $F^{16}(c_2,\alpha)$ and $F^{20}(c_1,\alpha)$ as a function of α in the subinterval of (α_c,α_1) which is indicated with brackets in (a). In both figures, the straight line indicates the location of the unstable fixed point p. The iterates $F^{l+m}(c_1)$ "follow" the iterates $F^l(c_2)$, while the signs defined in Eq. (8) satisfy $s_{l+m}(c_1)=-s_l(c_2)$. Thus, homoclinic crossings occur in pairs of contact-making $[s_l(c_2)>0]$ and contact-breaking $[s_{l+m}(c_1)<0]$ tangencies. This figure reveals the self-similar structure of the homoclinic tangency values. For this reason we expect antimonotonicity.

ages with the number of iterates k after which the preimage is mapped onto the unstable fixed point. The ordinate of these preimages on the graph corresponds to the actual location at the homoclinic tangency value. It is clear that for each of these values, at which $F^{13+k}(c_1,\alpha)=p$, the tangency is contact breaking, but there is another value nearby at which $F^{9+k}(c_2,\alpha)=p$ and the tangency is contact making. We expect the existence of infinitely many of these pairs.

We illustrate with Fig. 4 another way of looking at these pairs of homoclinic crossings. We have plotted in Fig. 4(a) the iterates $F^{15}(c_2,\alpha)$ and $F^{19}(c_1,\alpha)$ as functions of α for $\alpha\in(\alpha_c,\alpha_1)$, with α_c and α_1 the same as in Fig. 3 [$F^4(c_1,\alpha_c)=c_2$]. Figure 4(b) is an enlargement of Fig. 4(a) that corresponds to the subinterval of α values indicated in Fig. 4(a). We have plotted in Fig. 4(b) the iterates $F^{16}(c_2,\alpha)$ and $F^{20}(c_1,\alpha)$. In both figures, the straight line indicates the location of the unstable fixed point p. The figure shows that the occurrence of the pairs of homoclinic crossings is connected to the fact that both $F^{l+m}(c_1,\alpha)\cong F^l(c_2,\alpha)$ and $\partial F^{l+m}(c_1,\alpha)/\partial\alpha \cong \partial F^l(c_2,\alpha)/\partial\alpha$ for all $l\geq 1$, close to the parameter α_c at which $F^m(c_1,\alpha_c)=c_2$. Indeed we can see in Fig. 4 that, for parameter values close to α_c, the iterates $F^{l+4}(c_1)$ "follow" the iterates $F^l(c_2)$. Therefore, for each value at which $F^l(c_2)=p$, there is another one at which $F^{l+4}(c_1)=p$. Since this occurs while F^{13} is moving as in Fig. 3, then one of the tangencies is contact breaking and the other contact making. On the other hand, this figure also reflects the self-similar character of this kind of pictures with homoclinic tangency values accumulating on homoclinic tangency values. Therefore, we expect the existence of an infinite sequence of internested contact-making and contact-breaking homoclinic tangencies. This internested sequence will ultimately produce antimonotonicity.

V. SUPPORTING ANALYTICAL COMPUTATIONS

In this section we study analytically what happens to parameter values close to the one at which one critical point is mapped onto the other one. In particular, we develop a simplified model that shows how homoclinic tangencies occur in pairs as in Fig. 4 and that gives us estimates of the distances in parameter space between the corresponding homoclinic tangency values.

Let us call, as before, α_c the parameter value at which $F^m(c_1,\alpha_c)=c_2$. Without loss of generality, we take c_1 and c_2 to be independent of α. Thus, also at $\alpha=\alpha_c$, it is $\partial F^{r+m+1}(c_1,\alpha_c)/\partial\alpha=\partial F^{r+1}(c_2,\alpha_c)/\partial\alpha$ for all $r\geq 1$ [10]. As we are interested in values of α close to α_c, we will expand all quantities of interest assuming $\alpha\cong\alpha_c$. In this way, we get

$$F^m(c_1,\alpha)\cong c_2+\frac{\partial F^m(c_1,\alpha)}{\partial\alpha}(\alpha-\alpha_c)\ , \tag{2}$$

$$F^{m+r+1}(c_1,\alpha)\cong F^{r+1}(c_2,\alpha)+\frac{1}{2}\frac{\partial^2 F^{r+1}(c_2,\alpha)}{\partial x^2}\left[\frac{\partial F^m(c_1,\alpha_c)}{\partial\alpha}\right]^2(\alpha-\alpha_c)^2\ , \tag{3}$$

for all $r\geq 1$.

We now suppose that at $\alpha=\alpha_1$, there is a homoclinic tangency such that $F^{r+1}(c_2,\alpha_1)=p$ for some $r\geq 1$. We want to determine if there is a value α_2 at which $F^{r+m+1}(c_1,\alpha_2)=p$. For this reason we consider Eq. (3) at $\alpha=\alpha_2$ and insert in it the expansion

$$F^{r+1}(c_2,\alpha_1)\cong F^{r+1}(c_2,\alpha_1)+\frac{\partial F^{r+1}(c_2,\alpha_1)}{\partial\alpha}(\alpha_2-\alpha_1)$$
$$=p+\frac{\partial F^{r+1}(c_2,\alpha_1)}{\partial\alpha}(\alpha_2-\alpha_1)\ .$$

Taking into account that α_2 is such that $F^{r+m+1}(c_1,\alpha_2)=p$, then we obtain, to lowest order in $\alpha_1-\alpha_c$,

$$\alpha_2-\alpha_1\cong-\frac{1}{2}\frac{\dfrac{\partial^2 F^{r+1}(c_2,\alpha_c)}{\partial x^2}\left|\dfrac{\partial F^m(c_1,\alpha_c)}{\partial\alpha}\right|^2}{\dfrac{\partial F^{r+1}(c_2,\alpha_c)}{\partial\alpha}}(\alpha_1-\alpha_c)^2\ . \tag{4}$$

We can further simplify Eq. (4). First we use the equality

$$\frac{\partial^2 F^{r+1}(c,\alpha)}{\partial x^2}=\frac{\partial^2 F(c,\alpha)}{\partial x^2}\frac{\partial F^r(F(c,\alpha),\alpha)}{\partial x} \tag{5}$$

which holds for any critical point c and all $r\geq 1$. Then, as we did in Ref. [10], we use the positive Lyapunov exponent λ at the nearby chaotic parameter value α^*, to estimate the size of the spatial derivative at the critical value $w=F(c)$ as $\partial F^r(w,\alpha)/\partial x\approx C\exp(r\lambda)$ for r sufficiently large. Also, since $\partial F/\partial\alpha$ is bounded on the attractor, using this approximation for $\partial F^r(w,\alpha)/\partial x$, it is reasonable to assume that

$$\frac{\partial F^{r+1}(c,\alpha)}{\partial\alpha}=\frac{\partial F(F^r(c,\alpha))}{\partial\alpha}+\frac{\partial F(c,\alpha)}{\partial\alpha}\frac{\partial F^r(w,\alpha)}{\partial x}$$
$$\cong\frac{\partial F(c,\alpha)}{\partial\alpha}\frac{\partial F^r(w,\alpha)}{\partial x}$$
$$\approx C\frac{\partial F(c,\alpha)}{\partial\alpha}\exp(r\lambda)\ .$$

Introducing all these approximations in Eq. (4) we obtain

$$\alpha_2-\alpha_1\cong-\frac{1}{2}\frac{\dfrac{\partial^2F(c_2,\alpha_c)}{\partial x^2}\left|\dfrac{\partial F^m(c_1,\alpha_c)}{\partial\alpha}\right|^2}{\dfrac{\partial F(c_2,\alpha_c)}{\partial\alpha}}(\alpha_1-\alpha_c)^2 . \tag{6}$$

In order to determine whether the parameter α_2 of Eq. (6) is also close to α_c, we need to specify better what we mean by "sufficiently close" to α_c. We require that $\delta(\alpha)\equiv F^{m+1}(c_1,\alpha)-F(c_2,\alpha)$ and $\partial\delta/\partial\alpha$ provide only small corrections to the values that $F^{m+1}(c_1,\alpha)$ and $\partial F^{m+1}(c_1,\alpha)/\partial\alpha$ take on at $\alpha=\alpha_c$, i.e., $|\delta(\alpha)|\ll|F(c_2,\alpha)|$ and $|\partial\delta(\alpha)/\partial\alpha|\ll|\partial F(c_2,\alpha)/\partial\alpha|$. This also guarantees the validity of the truncations we have made of the Taylor expansions. Using Eq. (3) for $r=0$, its derivative to lowest order in $(\alpha-\alpha_c)$ and the estimates in terms of the Lyapunov exponent which we described before, we obtain that this criterion is satisfied if

$$|\alpha-\alpha_c|\ll\frac{\left|\dfrac{\partial F(c_2,\alpha_c)}{\partial\alpha}\right|}{\left|\dfrac{\partial^2F(c_2,\alpha_c)}{\partial x^2}\right|\left[\dfrac{\partial F^m(c_1,\alpha_c)}{\partial\alpha}\right]^2} . \tag{7}$$

If $\alpha=\alpha_1$ satisfies condition (7), it is easy to show that α_2 satisfies it as well. Therefore, if there is a homoclinic tangency at $\alpha=\alpha_1$ close to α_c such that $F^{r+1}(c_2,\alpha_1)=p$, there is another one at $\alpha=\alpha_2$ also close to α_c at which $F^{r+m+1}(c_1,\alpha_2)=p$.

We have compared the estimate (6) with the actual differences obtained for the pairs of homoclinic tangencies shown in Fig. 4, which correspond to the numerical example described in the preceding section. We have plotted in Fig. 5 the actual values of $\alpha_2-\alpha_1$ as a function of

$$-\frac{1}{2}\frac{\dfrac{\partial^2F(c_2,\alpha_c)}{\partial x^2}\left|\dfrac{\partial F^m(c_1,\alpha_c)}{\partial\alpha}\right|^2}{\dfrac{\partial F(c_2,\alpha_c)}{\partial\alpha}}(\alpha_1-\alpha_c)^2 .$$

For this example it is

$$\alpha_c=1.019\,398\,0 ,$$

$$m=4,\partial^2F(c_2,\alpha_c)/\partial x^2=-1.629 ,$$

$$\partial F^m(c_1,\alpha_c)/\partial\alpha=-5.811 ,$$

and

$$\partial F(c_2,\alpha_c)/\partial\alpha\cong83.33 .$$

The crosses that appear in Fig. 5(a) correspond to the five pairs of tangencies of Fig. 4(a) and those of Fig. 5(b) to the five pairs of tangencies of Fig. 4(b). We have also plotted the diagonal on Figs. 5(a) and 5(b). Provided that Eq. (6) is correct, the crosses should lie on the diagonal. First of all we see that the sign given by Eq. (6) is the correct one. On the other hand, we also see that Eq. (6) gives a good approximation of the value of α_2, even for values of α_1 that do not satisfy condition (7). For example, the last cross of Fig. 5(a) corresponds to $\alpha_1-\alpha_c\cong6\times10^{-6}$ while the right-hand side of Eq. (7) is 8.5×10^{-6}. However, the error introduced by using Eq. (6) instead of the actual values is less than 20%. This error can be further reduced if we use Eq. (5). We also see that, as expected, the approximation given by Eq. (6) is better as we approach the value of α_c. We can conclude then that the simplified model is in good agreement with what we find in our numerical example.

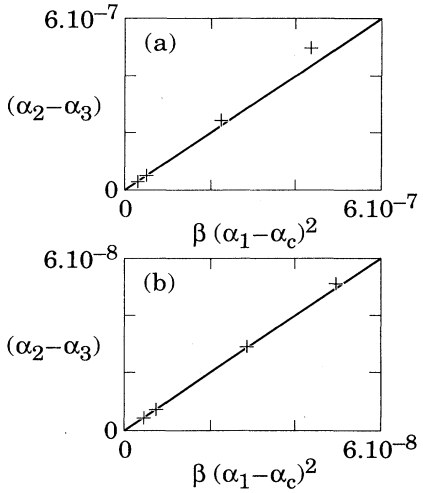

FIG. 5. (a) The values of $\alpha_2-\alpha_1$ obtained from Fig. 4(a) as a function of $\beta(\alpha_1-\alpha_c)^2$ (crosses) where $\beta=-\frac{1}{2}[(\partial^2F(c_2,\alpha_c)/\partial x^2|\partial F^m(c_1,\alpha_c)/\partial\alpha|^2/\partial F(c_2,\alpha_2)/\partial\alpha$. For this example, at $\alpha=\alpha_c=1.019\,398\,0$ it is $F^4(c_1)=c_2$, at $\alpha=\alpha_1$ it is $F^l(c_2)=p$ (for some $l>1$ and at $\alpha=\alpha_2$, $F^{l+4}=p$). (b) Similar to (a) but for the tangencies of Fig. 4(b). In both figures the cross that corresponds to the first pair of crossings is almost at the origin. The diagonal corresponds to the approximate value of $\alpha_2-\alpha_1$ as given by Eq. (6). We see that this formula gives a good estimate of $\alpha_2-\alpha_1$ that improves as we get closer to α_c.

We want to see now which type of tangencies occur at α_2 and α_1. For this reason we compute the sign

$$s_l(c,\alpha)\equiv-\mathrm{sgn}\left[\frac{\partial^2F^l}{\partial x^2}(c,\alpha)\frac{\partial F^l}{\partial\alpha}(c,\alpha)\right] \tag{8}$$

at $\alpha=\alpha_2$ for $l=r+m+1$ and $c=c_1$ and at $\alpha=\alpha_1$ for $l=r+1$ and $c=c_2$. If this sign is positive at the tangency, then the tangency is contact-making [as in the case of c being a maximum of F^l while $\partial F^l(c,\alpha)/\partial\alpha>0$]. If it is negative instead, it is contact-breaking. In order to calculate $\partial^2F^l/\partial x^2$ we use Eq. (5) where we insert the expansion (2). In order to calculate $\partial F^l/\partial\alpha$ we simply derive Eq. (3) with respect to α. In this way we get, to lowest order in $\alpha-\alpha_c$,

$$s_{r+m+1}(c_1,\alpha)\approx s_{r+1}(c_2,\alpha)s_m(c_1,\alpha)\mathrm{sgn}(\alpha-\alpha_c) . \tag{9}$$

Indeed, this equation reflects the fact that $s_{r+m+1}(c_1,\alpha)$ vanishes at $\alpha=\alpha_c$, something that occurs because $\partial^2F^{r+m+1}(c,\alpha)/\partial x^2$ vanishes whenever the critical point

c is mapped to a critical point.

For the purpose of the argument, suppose that for $\alpha<\alpha_c$ it is $s_{r+m+1}(c_1,\alpha)=s_{r+1}(c_2,\alpha)$. This holds if $s_m(c_1,\alpha)=-1$. Suppose that there are homoclinic tangencies for both $\alpha>\alpha_c$ and $\alpha<\alpha_c$. We consider then a homoclinic tangency that occurs at $\alpha_1>\alpha_c$. Then, by Eqs. (7) and (6), α_2 is also greater than α_c. If the stable set of the fixed point p is dense on the chaotic attractor at $\alpha=\alpha_c$, then it is always possible to choose r large enough so that α_1 and α_2 are so close to α_c that $s_m(c_1)$ does not vanish on $(\alpha_c,\max[\alpha_1,\alpha_2])$ [12]. Due to the same argument we also expect that $s_{r+1}(c_2)$ will not vanish for α between α_1 and α_2. In this way, one of the homoclinic tangencies will be contact making and the other contact breaking. Thus, we will have the creation and the destruction of periodic orbits for parameters nearby.

VI. CONCLUSIONS

We have presented a geometric mechanism for the creation and destruction of periodic orbits in families of chaotic scalar maps with at least two critical points c_1 and c_2 that satisfy certain typical conditions (excluding, for example, bimodal antisymmetric maps and maps which are the second or higher iterates of unimodal ones). We have proposed that a dimple formation mechanism, which can occur in a neighborhood of homoclinic tangency parameter values of multimodal maps, is the source of concurrent contact-making and contact-breaking homoclinic tangencies. Thus, this dimple formation is a geometric mechanism for antimonotonicity for generic families of maps $x_{n+1}=F(x_n,\alpha)$ for which there is a value α^* at which the attractor is chaotic and contains two critical points c_1 and c_2 in its interior.

We have illustrated the dimple formation mechanism in a detailed numerical study of a family of nonsymmetric cubic maps [see Eq. (1)]. A similar behavior is observable in the family

$$x_{n+1}=\alpha[-x_n^3+3(0.95)^2x_n]+C$$

with fixed α and variable C (see, e.g., Ref. [13]).

Our study of antimonotonicity in one-dimensional maps shows close similarities with the two-dimensional case. Unlike the two-dimensional case, however, there remain major mathematical difficulties which, presently, prevent us from constructing a rigorous proof of antimonotonicity in scalar maps. Nevertheless, the numerical examples we found, the analogy between the one- and the two-dimensional cases [13] and the geometrical mechanism we described in this paper provide support for the presence of antimonotonicity in generic families of chaotic scalar maps with at least two critical points.

ACKNOWLEDGMENTS

We would like to thank I. Kan for extensive useful conversations. We also gratefully acknowledge the financial support from the Consejo Nacional de Investigaciones Científicas y Técnicas (Argentina), NSF, AFOSR, and the U.S. Department of Energy (Office of Scientific Computing, Office of Energy Research).

[1] M. Feigenbaum, J. Stat. Phys. **19**, 25 (1978).

[2] N. Metropolis, M. L. Stein, and P. R. Stein, J. Combin. Theory **15**, 25 (1973).

[3] J. P. Gollub, S. V. Benson, and J. F. Steinman, Ann. N.Y. Acad. Sci. **357**, 22 (1980); A. Libchaber and J. Maurer, J. Phys. (Paris) Colloq. **41**, C3-51 (1980); M. Giglio, S. Musazzi, and U. Perrini, Phys. Rev. Lett. **47**, 243 (1981); A. Libchaber, C. Laroche, and S. Fauve, J. Phys. (Paris) Lett. **43**, L211 (1982); P. S. Linsay, Phys. Rev. Lett. **47**, 1349 (1981); E. R. Hunt and R. W. Rollins, Phys. Rev. A **29**, 1000 (1984); T. T. Arecchi, R. Meucci, G. Puccioni, and J. Tredicce, Phys. Rev. Lett. **49**, 1217 (1982).

[4] J. Milnor and P. Thurston, in *Dynamical Systems,* edited by J. C. Alexander, Lecture Notes in Mathematics Vol. 1342 (Springer-Verlag, Berlin, 1988), p. 465.

[5] U. Parlitz and W. Lauterborn, Phys. Lett. A **107**, 351 (1985); U. Parlitz and W. Lauterborn, Phys. Rev. A **36**, 1428 (1987).

[6] H. L. Swinney, Physica D **7**, 3 (1983); K. Coffman, W. D. McCormick, and H. L. Swinney, Phys. Rev. Lett. **56**, 999 (1986).

[7] J. Guckenhemier, Physica D **1**, 227 (1980); L. Glass and R. Pérez, Phys. Rev. Lett. **48**, 1772 (1982); J. Grasman, N. Nijmeijer, and J. M. Veiling, Physica D **13**, 195 (1984); R. S. Mackay and C. Tresser, *ibid.* **19**, 206 (1986).

[8] C. Scheffczyk, U. Parlitz, T. Kruz, W. Knop, and W. Lauterborn, Phys. Rev. A **43**, 6495 (1991); J. Ringland, N. Issa, and M. Schell, *ibid.* **41**, 4223 (1990); S. Fraser and R. Kapral, *ibid.* **25**, 3223 (1982); R. S. Mackay and C. Tresser, Physica D **27**, 412 (1987); S-J Chang, M. Wortis, and J. A. Wright, Phys. Rev. A **24**, 2669 (1981); J. Coste and N. Peyraud, Physica D **5**, 415 (1982).

[9] I. Kan, H. Koçak, and J. A. Yorke, Ann. Math. **136**, 219 (1992).

[10] S. P. Dawson, C. Grebogi, I. Kan, H. Koçak, and J. A. Yorke, Phys. Lett. A **162**, 249 (1992).

[11] R. Devaney, *An Introduction to Chaotic Dynamical Systems* (Benjamin/Cummings, Menlo Park, CA, 1986), p. 121.

[12] In particular, we think that this will hold if there are no stable periodic orbits of period less than $m+1$ for parameters values in $(\alpha_c,\max[\alpha_1,\alpha_2])$ and of period less than $r+1$ for parameters between α_2 and α_1.

[13] S. P. Dawson and C. Grebogi, Chaos, Solitons and Fractals **1**, 137 (1991).